Effect of gedunin on glioblastoma proliferation and invasiveness: *in vitro* and *in vivo* approaches

Thadeu Estevam Moreira Maramaldo Costa[a,b,*], Tatiana Almeida Pádua[b], Jonathas Xavier Pereira[c], Vinicius Gonçalves Rodrigues[c], Leonardo Noboru Seito[b], Erika Marques da Cunha[b], Claudio C. Filgueiras[d], Yael Abreu-Villaça[d], Alex C. Manhães[d], Clarissa Menezes Maya-Monteiro[e], Maria das Graças Henriques[b,f], Thomas Eichenberg Krahe[d,g], Carmen Penido[a,b]

[a] Centro de Desenvolvimento Tecnológico em Saúde, Instituto Nacional de Ciência e Tecnologia de Inovação em Doenças Negligenciadas (INCT-IDN), Fundação Oswaldo Cruz, Rio de Janeiro, Brazil.

[b] Laboratório de Farmacologia Aplicada, Instituto de Tecnologia em Fármacos (Farmanguinhos), Fundação Oswaldo Cruz, Rio de Janeiro, Brazil.

[c] Instituto de Patologia Tropical e Saúde Pública (IPTSP), Universidade Federal de Goiás (UFG), Goiás, Goiânia, Brasil.

[d] Laboratório de Neurofisiologia, Departamento de Ciências Fisiológicas, Instituto de Biologia Roberto Alcantara Gomes, Universidade do Estado do Rio de Janeiro (UERJ), Rio de Janeiro, Brazil.

[e] Laboratório de Imunofarmacologia, Instituto Oswaldo Cruz (IOC), Fundação Oswaldo Cruz, Rio de Janeiro, Brazil.

[f] Laboratório de Farmacologia Celular e Molecular, Departamento de Biologia Celular; Instituto de Biologia Roberto Alcântara Gomes, Universidade do Estado do Rio de Janeiro (UERJ), Rio de Janeiro, Brazil.

[g] Departamento de Psicologia, Pontifícia Universidade Católica do Rio de Janeiro (PUC-Rio), Rio de Janeiro, Brazil.

[*]**Address correspondence to**: Dr. Thadeu Costa, Laboratório de Farmacologia Aplicada, Departamento de Farmacologia Aplicada, Farmanguinhos, Fundação Oswaldo Cruz, Rua Sizenando Nabuco 100, Manguinhos, Rio de Janeiro, RJ, CEP 21041-250, Brazil, e-mail: thadeu.costa@fiocruz.br.

41 **Graphical Abstract**

42

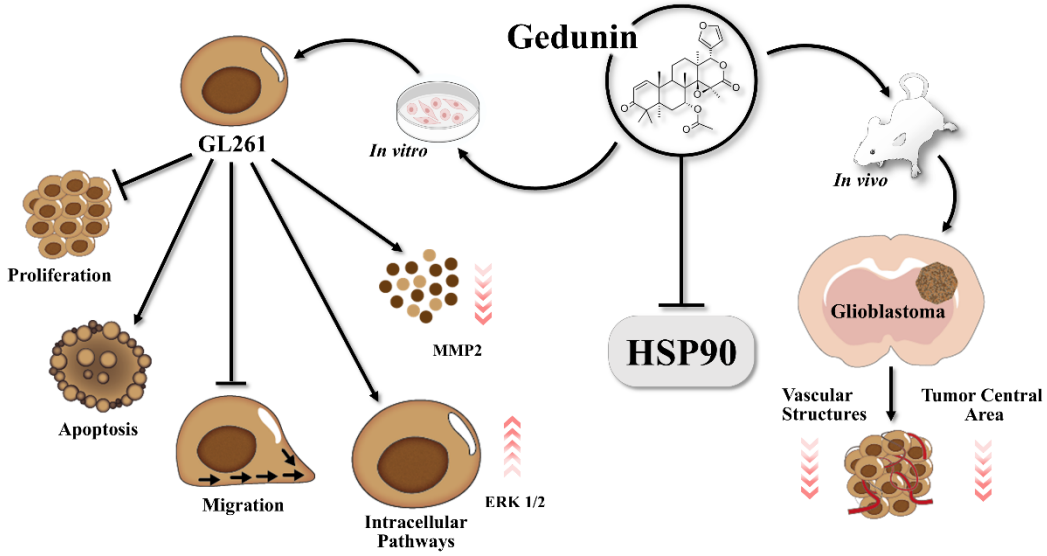

43

44

45

46 **Abstract (250 palavras)**

47 **Background** Glioblastoma is the most invasive and malignant brain tumor, for which no
48 effective treatment is currently available. Heat shock protein 90 (HSP90) is a potential
49 target for the treatment of different types of cancer. Herein, we investigated the effect of
50 gedunin, an HSP90 inhibitor, in murine GL261 glioblastoma *in vitro* and *in vivo* models.
51 **Methods:** Gedunin effects were assessed by *in vitro* cell viability assay (MTT), apoptosis
52 (PI/Annexin staining), proliferation (CFSE), invasion (transmigration, scratch assay and
53 zymography), protein detection (western blot) and *in vivo* orthotopic glioblastoma model
54 (brain computed tomography and histology)**. Results:** Gedunin treatment decreased
55 GL261 cell proliferation and triggered apoptosis in a concentration-dependent manner.
56 Gedunin also reduced GL261 cell migration and metalloproteinase-2 activity, suggesting
57 that it impairs glioblastoma cell invasion. Despite the reduction of total protein content in
58 gedunin-treated cells, the phosphorylation of STAT3 and ERK1/2 pathways was
59 enhanced within 24 h. *In situ* treatment with gedunin did not significantly reduce tumor
60 volume. Still, it reduced the tumor central area and the presence of vascular structures in
61 xenograft glioblastoma in C57BL/6 mice, a clinical feature associated with morbidity and

mortality. **Conclusion:** Gedunin inhibits murine glioblastoma cell growth and proliferation by inducing apoptosis.

Keywords: Brain tumor, GL261, limonoids, natural products.

List of abbreviations

17-AAG - 17-(Allylamino)-17-demethoxygeldanamycin/tanespimycin
AKT/PKB - protein kinase B
ARRIVE - Animal Research: Reporting of *In Vivo* Experiment
BCR/ABL - breakpoint cluster region/Abelson murine leukemia virus
CFSE - carboxyfluorescein succinimidyl ester
DMEM - Dulbecco´s modified Eagle´s medium
DMSO - dimethyl sulfoxide
EDTA - ethylenediamine tetraacetic acid
Erk ½ - extracellular signal-regulated kinases ½
FBS - Fetal bovine serum
FITC - fluorescein isothiocyanate
GAPDH - glyceraldehyde-3-phosphate dehydrogenase mouse
HER2/neu, ErbB2 - human epidermal growth factor receptor 2
HPF - high-power fields
HSP90 – Heat Shock Protein 90
IgG – immunoglobulin G
MMP - matrix metalloproteinase
MTT - 3-(4,5-dimethyl-2-thiazolyl)-2,5-diphenyl-2H-tetrazolium bromide
p44/42 MAPK - mitogen-activated protein kinase
PBS - phosphate buffer saline
PI -propidium iodide
SDS-PAGE - sodium dodecyl sulfate-polyacrylamide gel electrophoresis
Src - proto-oncogene c-Src

1. Introduction

Glioblastoma is a highly invasive and malignant tumor defined by the World Health Organization as grade IV, based on histological, immunohistochemical, and molecular features [1]. Patients bearing glioblastoma have a poor prognosis, with estimated median survival rates of eight months and a maximum five-year survival rate of only 5% [2,3].

The current standard protocol for glioblastoma treatment relies on total tumor excision followed by radiotherapy with concurrent and adjuvant chemotherapy with temozolomide [4]. The most common adverse events related to temozolomide treatment are myelosuppression and hepatotoxicity [5–7]. Another limiting factor of glioblastoma treatment is that most orally and intravenously administered alkylating agents induce resistance and have poor blood-brain barrier permeability [8,9]. An alternative strategy is the usage of intracranial wafer implants containing the alkylating agent carmustine after tumor removal surgery, which, in combination with radiochemotherapy, has been shown to significantly improve patient survival [10,11]. However, carmustine wafers induce severe side effects, such as cerebral edema and hematological toxicity [5,12,13]. Glioblastoma is still considered incurable [14]; however, treatments targeting multiple signaling pathways are a promising strategy [15].

Modulation of the chaperone heat shock protein 90 (HSP90) is considered a potential antitumor therapy, including gliomas [16–18]. HSP90 activity is implicated in several hallmarks of cancer, such as proliferation, invasion, metastasis, angiogenesis, and resistance to apoptosis [19]. Increased expression of HSP90 correlates with tumor malignancy and poor prognosis in different types of cancer, including breast, colon, and melanoma [20–23]. Indeed, HSP90 chaperones several proteins involved in oncogenic processes, including the human epidermal growth factor receptor 2 (HER2/neu; ErbB2), tyrosine-protein kinase Src (Src), protein kinase B (AKT/PKB), breakpoint cluster region/Abelson murine leukemia virus (BCR/ABL) and tumor protein 53 (p53) [24–26]. In line with this, encouraging pre-clinical data have been obtained with HSP90 inhibitors in different types of tumor cells and animal models, including lymphoma, melanoma, breast, and lung cancer [27–31]. Currently, in the National Institutes of Health (NIH) Clinical Trials database at ClinicalTrials.gov, there are more than a hundred registered trials (11 currently active) evaluating HSP90 inhibitors (alone or in combination with

other drugs) for the treatment of different types of cancer [32]. Worthy of note, off-target toxicity, including ocular toxicity and hepatotoxicity, is a limiting factor for the use of these substances [33,34].

Over the past two decades, our group and others have been studying the antitumoral and anti-inflammatory effects of gedunin, a limonoid produced by vegetal species from the Meliaceae family [35] or by semi-synthetic routes [36]. Gedunin negatively modulates HSP90 activity by binding to the HSP90 co-chaperones p23 and cdc37 and, thus, impairing the formation of the active HSP90 complex [37,38]. This limonoid has potent antitumoral effects demonstrated against an array of tumor types *in vivo* and *in vitro* [37,39–42]. Gedunin anti-tumoral effect on glioblastoma has been shown *in vitro* human cells lines U87 and U251 [43,44]. However, this effect has been observed in only a few studies using cell lines. Therefore, further efforts are needed to reproduce previous findings and to further investigate the anti-glioblastoma effect of gedunin in an *in vivo* model. In the present study, we used the murine GL261 cell line in *in vitro* assays to translate the data obtained *in vitro* to a syngeneic *in vivo* model, using the well-established orthotopic *in vivo* glioblastoma model.

142 **2. Materials and Methods**

143 ***2.1 Reagents and antibodies***

144 Gedunin (Gaia Chemicals, USA) and the specific HSP90 inhibitor 17-AAG (17-N-
145 allylamino-17-demethoxygeldanamycin, Tanespimycin, Sigma-Aldrich, USA) were
146 dissolved in DMSO (dimethyl sulfoxide, Sigma-Aldrich) and frozen at -86 °C until use.
147 MTT (3-(4,5-dimethylthiazol-2-yl)-2,5-diphenyl tetrazolium bromide), Dulbecco´s
148 modified Eagle´s medium (DMEM), phosphate buffer saline (PBS) tablet, and trypsin-
149 EDTA (ethylenediamine tetraacetic acid) solution were purchased from Sigma Aldrich.
150 Fetal bovine serum (FBS) was purchased from Cultilab (Brazil). Propidium iodide (PI)
151 solution was obtained from Biolegend (USA). Vybrant™ CFDA-SE (carboxyfluorescein
152 diacetate succinimidyl ester) Cell Tracer Kit and gentamicin were obtained from Thermo
153 Fischer Scientific (USA). Annexin V-FITC (fluorescein isothiocyanate) conjugated was
154 purchased from BD Pharmingen (USA). Antibodies against rabbit p44/42 MAPK
155 (mitogen-activated protein kinase, Thr202/Tyr204, D13.14.4E), ERK1/2 (extracellular
156 signal-regulated kinase 1/2, rabbit) and GAPDH (glyceraldehyde-3-phosphate
157 dehydrogenase mouse, D4C6R) were purchased from Cell Signaling (USA). Anti-rabbit-
158 IgG-HRP (horseradish peroxidase) secondary antibody was purchased from Santa Cruz
159 Biotechnologies (USA). DNase I recombinant RNase free was purchased from Roche
160 Life Sciences (Germany).

161

162 ***2.2 GL261 cell culture and treatment***

163 Murine glioblastoma cell line (GL261, Cell Bank from Federal University of Rio de
164 Janeiro - UFRJ, Brazil) was cultured in DMEM (Sigma Aldrich) supplemented with 10
165 % FBS (Cultilab) and 50 µg/mL gentamicin (Thermo Fisher Scientific) in humidified
166 atmosphere (5 % CO_2 at 37 °C) until confluence. Cells were digested with 0.25 % trypsin
167 at the 5th passage and washed with 1 × PBS. Cell viability was determined by trypan blue
168 (Sigma Aldrich) staining under a light microscope, before further assays. GL261 cells
169 were incubated with 6.25-100 µM of gedunin for 24-72 h at 37 °C, 5 % CO_2.

170

171 ***2.3 Animals***

172 Adult male C57BL/6 mice (20-25 g) provided by Oswaldo Cruz Foundation (Fiocruz)
173 breeding unit (Institute for Biomodels Science and Technology, Rio de Janeiro, Brazil)

were kept in standard autoclavable polypropylene boxes, with free access to food and fresh water in environmentally controlled room temperature (ranging from 22 to 24 °C) on a light/dark cycle at Farmanguinhos (Fiocruz, Rio de Janeiro, Brazil) and at the Laboratory of Neurophysiology (State University of Rio de Janeiro, Rio de Janeiro, Brazil) experimental animal facilities. Animal procedures were performed in accordance with the ethical guidelines of the Brazilian National Council for the Control of Animal Experimentation (CONCEA) and reported following the ARRIVE guidelines [45]. Experimental procedures were approved by the Ethics Commission on Animal Use of Oswaldo Cruz Foundation (license #LW-35/16) and the Ethics Commission on Animal Use of the State University of Rio de Janeiro (license #025/2017).

2.4 Primary mixed glial cell culture

Under sterile conditions, mouse brain cortex tissue was rapidly dissected from euthanized (150 mg/kg sodium thiopental, i.p.) young adult (4-week-old) C57BL/6 male mice and transferred to ice-cold DMEM/F12 media (Sigma Aldrich) in 6 well plates. After removal of the meninges, brain tissue was cut into small pieces, and washed three times with 1x sterile PBS (Sigma Aldrich). Trypsin-DNAse solution (0.25 % - 250 µg/mL) was added to the wells and the plate was incubated for 1 h in an orbital shaker (Excella E24, New Brunswick Scientific, USA) at 37 °C and 150 rpm. Tissue samples were vigorously triturated and dissociated with a 1 mL pipette tip. Cells were washed with FBS-DNAse solution (10 % - 250 µg/mL), added to a 20 % percoll gradient media, and centrifuged at 800 × *g* for 30 min at 25 °C. Recovered cells were washed (400 × *g*, 10 min at 4 °C), distributed in T-25 bottle flasks, and incubated at 37 °C, 5 % CO_2. DMEM/F12 media was changed every 3-4 days until use. Data were collected from two independent experiments (n=5 mice per group; license #LW-35/16).

2.5 Proliferation assay

GL261 cells (4×10^7/mL) were incubated with 5 µM CFSE solution (Invitrogen Molecular Probes, USA) diluted in PBS for 15 min at 37 °C, 5 % CO_2. Cells were washed with 10 % PBS/FBS solution, seeded in 24 well plates (2×10^5 cells per well), incubated overnight, and treated with gedunin (6.25-100 µM) for 72 h. Cell proliferation was evaluated by analyzing CFSE fluorescence intensity (FL1) upon cell divisions, by flow

206 cytometry (FACScalibur, Becton Dickinson, USA). Results were analyzed using FlowJo
207 X Software (Tree Star, Becton Dickinson).
208
209 ***2.6 MTT assay***
210 GL261 or primary mixed glial cells were seeded in a 96 flat bottom well plate (2×10^4
211 cells/well) and cultured in DMEM for 24 h (CO_2 5 % at 37 °C) for adhesion. Adherent
212 cells were cultured with different concentrations of gedunin (6.25-100 μM), 17-AAG (1
213 μM), or temozolomide (100 μM) for 20 or 68 h, when MTT solution (5 mg/mL; 22.5
214 μL/well) was added to the culture and incubated for 4 h. The analyzes were performed at
215 24 and 72 h time points. Plates were centrifuged for 3 min (720 × *g* at 4 °C), the
216 supernatant was discharged and DMSO (150 μL/well) was added for formazan crystals
217 solubilization. The absorbance was read in a microplate reader (SpectraMax M5,
218 Molecular Devices, USA) at 540 nm.
219
220 ***2.7 Determination of apoptosis***
221 Apoptosis was evaluated using annexin V-FITC and propidium iodide (PI) staining.
222 GL261 cells were seeded in 24 well cell culture plates (2×10^5 cells/well) and left to
223 adhere overnight. GL261 cells were then incubated with gedunin (6.25 - 100 μM) for 24
224 or 72 h, followed by trypsinization, resuspension in annexin V Binding Buffer (HEPES
225 10 mM pH 7.4, NaCl 140 mM, $CaCl_2$ 2.5 mM) and labeling with annexin V-FITC and PI
226 for 15 min at room temperature. Cells incubated with medium were used as the negative
227 control, whereas 17-AAG-incubated cells were used as the positive control. Staining was
228 analyzed by cytometry using FACScalibur (Becton Dickinson) and FlowJo Software
229 (Tree Star, Becton Dickinson). At least 10^4 cells were acquired per sample. Data are
230 presented in dot plots in a log scale of increasing FL-1 (annexin V-FITC) and FL-3 (PI)
231 intensity.
232
233 ***2.8 Scratch assay***
234 GL261 cell monolayers, seeded into 6 well plates, were scratched at the center of the well,
235 and then the migration path was assessed at the leading edge of the scratch by phase-
236 contrast optical microscopy (100 ×, Olympus IX70, Japan) at indicated time points.
237 Analyses were performed using Image J software (National Institute of Health, USA)

238 **[46]**. The rate of migration was determined by quantifying the total distance that cells
239 moved from the edge of the scratch toward the center of the scratch, as previously
240 described **[47]**.
241
242 ***2.9 Chemotaxis assay***
243 GL261 cell migration was assayed in a 48-well micro-chemotaxis Boyden chamber
244 (Neuro Probe Inc., USA). The bottom wells of the chamber were filled with DMEM 10
245 % FBS (29 μL) or serum-free DMEM media as the negative control. Polycarbonate
246 membrane filters with 8 μm pore size (Neuro Probe) were placed between the lower and
247 upper chambers. GL261 cells were pre-treated with different concentrations of gedunin
248 (6.25-25 μM) for 1 h in serum-free DMEM and then loaded into the upper wells of
249 Boyden chamber (2×10^4 cells/50 μL/well). The chamber was incubated in a humidified
250 atmosphere with 5 % CO_2 at 37 °C for 24 h. The membranes were removed and stained
251 using a Diff-quick (Laborclin, Brazil). The bottom side of the membranes was visualized
252 by light microscopy for counting GL261 migrating cells (1000 ×, Olympus IX70). GL261
253 chemotaxis was calculated and expressed as the mean number of migrated cells in ten
254 random high-power fields (HPFs) per well (in quadruplicate).
255
256 ***2.10 Zymography***
257 GL261 cells were plated (1×10^6/well) in a 6-well plate in DMEM. After 24 h,
258 supernatant was removed, and cells were washed 3 times with pure DMEM to eliminate
259 any FBS trace. Then, cells received gedunin (6.25-50 μM) or 17-AAG (1 μM) treatment
260 in serum-free DMEM. After 48 h, the supernatant was collected and stored at -70 °C until
261 lyophilization. Samples were dehydrated in a Gamma 2-16 LSCplus (Christ, Germany)
262 ice condenser and, resuspended with 200 μL of zymography extraction buffer (Tris-HCl
263 50 mM pH 7.5, NaCl 0.2 M, Triton X-100 0.1 %, $CaCl_2$ 10 mM, protease inhibitor
264 cocktail). Lowry method was used for protein quantitation. Enzymatic activity of matrix
265 metalloproteinase (MMP)-2 was determined on a 10 % SDS-PAGE containing 0.1 %
266 gelatin from porcine skin (Sigma Aldrich) [48].
267
268
269

270 ***2.11 Western blot***

271 GL261 cells (1 × 10^5 cells) treated with gedunin (6.25-100 μM) or 17-AAG (1 μM) for
272 24 h were lysed in a buffer containing protease inhibitors. Protein extract (20 μg) was
273 resolved by SDS-PAGE, proteins were transferred to polyvinylidene difluoride (PVDF)
274 membranes (GE Healthcare, USA), and then probed with primary antibodies. Antibodies
275 were diluted in Tris-buffered saline containing 0.5 % Tween 20 and 5 % non-fat milk or
276 bovine serum albumin (BSA, Sigma -Aldrich, USA), and incubated overnight at 4 °C.
277 The membranes were incubated with horseradish peroxidase (HRP)-conjugated
278 secondary IgG (Santa Cruz Biotechnology) for 1 h at room temperature. The blots were
279 developed in a Hyperfilm with the use of a chemiluminescent substrate (ECL; Amersham
280 Biosciences, USA). The band intensity was quantified using ImageJ (NIH, USA), and
281 expressed in arbitrary units (a.u.). The raw intensity values of total proteins were
282 normalized using the values of the constitutive protein (GAPDH, used as loading control)
283 and of the control group (untreated cells) to allow comparison between different
284 experiments. The phospho-protein values were normalized by the specific total protein
285 content. Western blot membranes were stripped using harsh stripping buffer (SDS 10%
286 Tris HCl, pH 6.8, 0.5 M; 0.8 % ß-mercaptoethanol), at 50 °C for up to 45 min under
287 agitation in an orbital shaker (Excella E24, New Brunswick Scientific, USA). Stripping
288 was performed between the phospho and total proteins antibody incubations. Analyses
289 were performed using Image J software (NIH, USA)**[46]**.

290

291 ***2.12 Orthotopic glioblastoma model and osmotic mini-pump implantation***

292 Glioblastoma was induced in adult male C57BL/6 by stereotaxic injections of GL261
293 cells at the Laboratory of Neurophysiology experimental animal facility (UERJ, Rio de
294 Janeiro, Brazil). Mice were intraperitoneally anesthetized with 100 mg/kg ketamine
295 (Syntec, Brazil) and 10 mg/kg xylazine (Sedalex™ Venco, Brazil). Under sterile
296 conditions, a midline incision was made in the scalp, the skull was exposed to identify
297 bregma and lambda, and a small burr hole was drilled over the right hemisphere. GL261
298 cells (5 × 10^4/μL; final volume of 2 μL) were stereotaxically injected into the caudate
299 putamen with a 10 μL Hamilton syringe at the rate of 0.5 μL/min. The needle was slowly
300 removed 4 min after the injection was finished. The following coordinates (in mm) were
301 used for stereotaxic injections (anterior-posterior; medial-lateral; dorsal-ventral): 0.1

302 AP; 2.32 ML; 2.35 DV. Coordinates were based on the Cha et al., 2003 [49] descriptions
303 and confirmed on Paxinos and Franklin mouse brain atlas [50]. Fourteen days after
304 GL261 injections, animals were implanted with Alzet osmotic minipumps (model 2004,
305 0.25 μL/h; Durect Corporation, USA) filled with gedunin (250 μM, n=8) or DMSO (2.5
306 %, n=8). Cannulas (1-2 mm long) were placed into the site of the tumor following similar
307 surgical procedures described above. Treatment lasted between 14 and 17 days. Mice
308 were monitored every day for clinical signs of pain and distress, such as ruffled fur,
309 hunched back, trembling, convulsions, paralysis, and permanent recumbency [51]. If
310 signs of pain and distress were observed, the animal was excluded from the study and
311 euthanized. Data were collected from two independent experiments (n=8 randomized
312 mice per group). Mice were euthanized 28 days after GL261 injection with sodium
313 thiopental (150 mg/kg, i.p.).
314
315 ***2.13 Mouse Brain Computed Tomography Images***
316 After 14-day treatment, anesthetized mice (100 mg/kg ketamine/10 mg/kg xylazine, i.p.)
317 were intravenously (i.v.) injected with 300 mg/mL of Omnipaque iohexol contrast (GE
318 Healthcare). Brains were scanned 3-6 min after contrast administration in a GE Highspeed
319 CT/E image system (Pedro Ernesto University Hospital, UERJ, Rio de Janeiro, Brazil),
320 according to the following protocol: 120 kV tube voltage, 55 mA, 1 mm slice thickness.
321 Images were reconstructed in a 256 x 256-pixel matrix using InVesalius 3.1.1 software
322 (developed by Centro de Tecnologia da Informação Renato Archer, CNPq, and Ministry
323 of Health, Brazil). Tumor volumetry was determined by selecting contrast-enhanced
324 regions of interest in coronal sections.
325
326 ***2.14 Histology of Brain Tissue***
327 Euthanized mice (150 mg/kg sodium thiopental, i.p.) were perfused with 4 %
328 formaldehyde. Mouse brains were collected and transferred into a 4 % formaldehyde
329 solution for 2 days for tissue fixation. Brains were then sectioned and embedded in
330 paraffin. Coronal sections of brain tissue (5 μm) were made using a Shandon Finesse 325
331 microtome (Thermo Fisher Scientific). Brain slices were stained with hematoxylin
332 (Merck, USA) and eosin (Sigma Aldrich, USA). Tumor central area was measured using
333 Axioplan® software [52]. Lesion size, liquefactive necrosis area, vascular structures,

intratumoral hemorrhage, and mitosis were blindly analyzed in the central slice tumor area. Lesion size area was defined by the percentage of tumor area relative to the size of the total brain area in the slice. The liquefactive necrosis area was determined by the percentage of necrosis area relative to lesion size. Vascular structures with their full composition were counted in both intratumor and peritumoral regions. Intratumor hemorrhage was described in a semi-quantitative form regarding the intensity at the slice, with the following definitions: discrete (+), moderate (++), and intense (+++). Mitosis was characterized by estimating the average amount of cells per analyzed field, and thus: >50% (+), 50-75% (++), and >75% (+++). Multipoint brain slice images were composed in NIS-Elements AR (Nikon Corporation). Each brain slice was analyzed by an observer blind to the experimental groups.

2.15 Statistical Analysis

All analyses were performed using GraphPad Prism 8 (GraphPad Software, USA). Western blot analyses were performed using the non-parametric Kruskal-Wallis test followed by Dunnett's multiple comparisons. Histologic analyses were performed by one-way analysis of variance (ANOVA) and Tukey's post-test for multiple comparisons. All other comparisons were carried out using one-way ANOVA followed by the Student-Newman-Keuls test. Data are shown as the mean $\pm$ SEM (unless otherwise mentioned). Significance was assumed either at the level of $p \leq 0.05$, $p \leq 0.01$, or $p \leq 0.001$, as specified.

356 **3. Results**

357 ***3.1 Gedunin impairs GL261 cell growth and viability in vitro***

358 To verify the effect of gedunin on GL261 cell growth, a 72 h CFSE proliferation assay
359 was performed, in which staining decreases as cells proliferate. Incubation of CFDA-SE-
360 stained GL261 cells with gedunin decreased cell proliferation in a concentration-
361 dependent manner (**Fig. 1A**). Gedunin (25-100 μM) significantly inhibited GL261 cell
362 growth, similar to what was observed with the selective HSP90 inhibitor 17-AAG
363 (reference control). **Figure 1B** shows representative histograms of CFSE fluorescence
364 intensity (FL-1) of GL261 cells depicted in **Figure 1A**.

365 The effect of gedunin on cell viability was evaluated by the MTT assay. The incubation
366 of GL261 cells with gedunin decreased mitochondrial function in a concentration-
367 dependent manner within 24 and 72 h (**Fig. 1C**). MTT assay was also performed on
368 primary mixed glial cells to evaluate gedunin toxicity to non-tumoral cells. Gedunin
369 effect on primary mixed glial cells was less toxic, and higher concentrations were required
370 to induce cell death when compared to GL261 cells (**Fig. 1C**). The half-maximal
371 inhibitory concentration [IC50] of gedunin on GL261 cells was 2.3 times lower than the
372 IC_{50} observed on primary glial cells (**Fig. 1D**). Temozolomide, the first-line treatment for
373 glioblastoma, also reduced GL261 viability within 72 h in a concentration-dependent
374 manner (**Suppl. Fig. 1**). Considering the antiproliferative and cytotoxic effects of gedunin
375 on GL261 cells, we further examined whether this limonoid induced apoptosis.
376

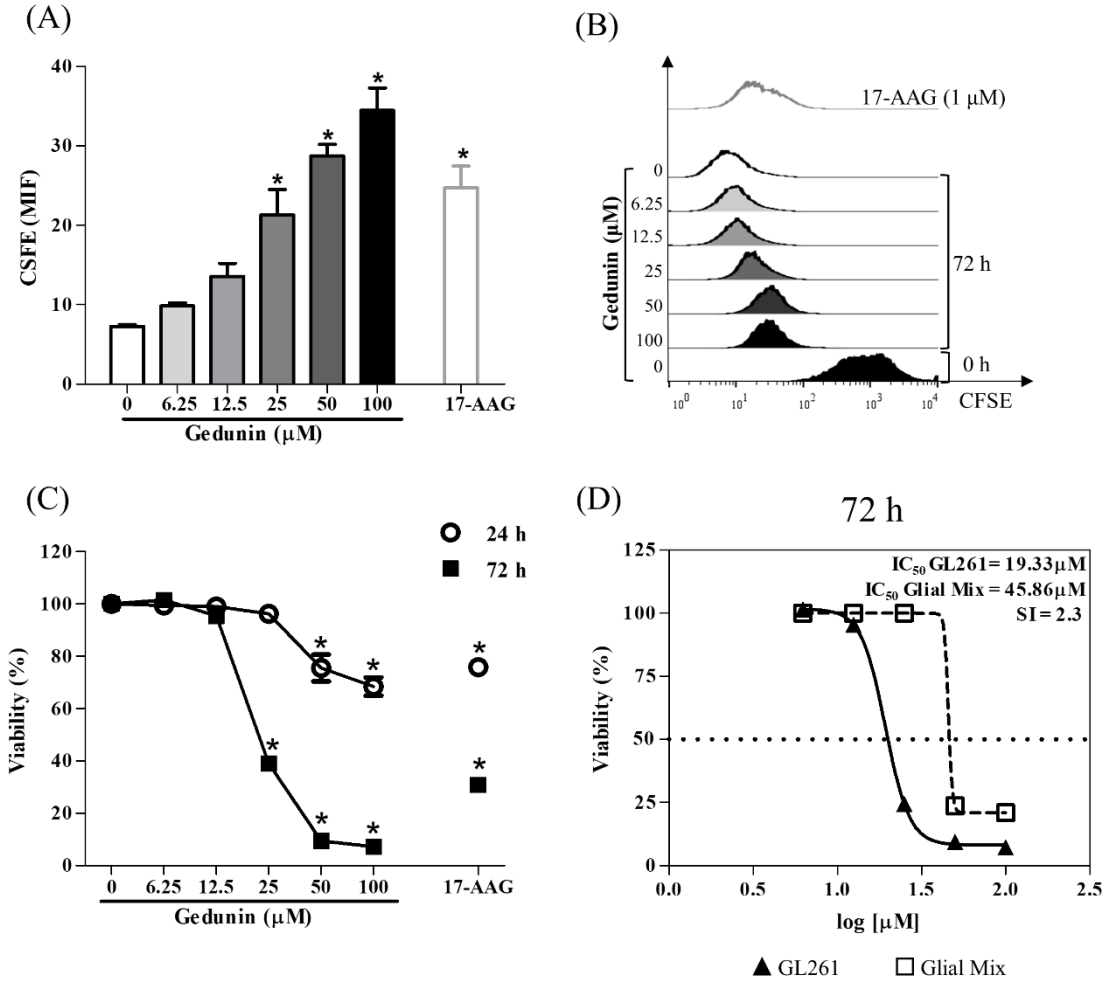

Figure 1. *Gedunin impairs GL261 cell proliferation.* (A) Effect of gedunin (6.25-100 μM) and 17-AAG (1 μM) on GL261 cell proliferation evaluated by CFSE staining and analyzed by FACScalibur (BD Biosciences) 72 h after incubation. Results are expressed as the mean ± SEM of median fluorescence intensity (MFI) from triplicate wells from three independent experiments. (B) Representative histogram shows CFSE fluorescence intensity (FL-1) from one experiment. (C) Effect of gedunin (6.25-100 μM) and 17-AAG (1 μM) on GL261 cell viability evaluated by MTT reduction assay (SpectraMax M5, Molecular Devices) 24 and 72 h after incubation. (D) IC50 values of gedunin treatment on GL261 and glial mixed cells 72 h after incubation. SI: selectivity index.

3.2 Gedunin induces GL261 cell apoptosis in vitro

Apoptosis is regulated by a series of signaling events that include disruption of the mitochondrial membrane and phosphatidylserine externalization [53,54]. Membrane

392 phosphatidylserine staining by annexin V-FITC revealed that gedunin induced apoptosis
393 of GL261 cells in a concentration- and time-dependent manner (**Fig. 2A**). Apoptosis was
394 detected 24 h after treatment, and surpassed 90 % within 72 h, at the highest
395 concentrations. Representative dot plots of PI^+ and annexin V^+ cells are shown in **Figure**
396 **2B**. Apoptotic cells are characterized by reduced forward scatter and increased side scatter
397 [55–57]. Indeed, GL261 cells incubated with gedunin diminished FSC-H and increased
398 SSC-H intensities, when compared to non-treated cells (**Fig. 2C**), supporting results
399 shown in Figures 2 A and B. Representative dot-plots of the effect of 17-AAG (1 μM) on
400 GL261 apoptosis (24 h and 72 h) is available on **Supplemental Figure 2**.
401

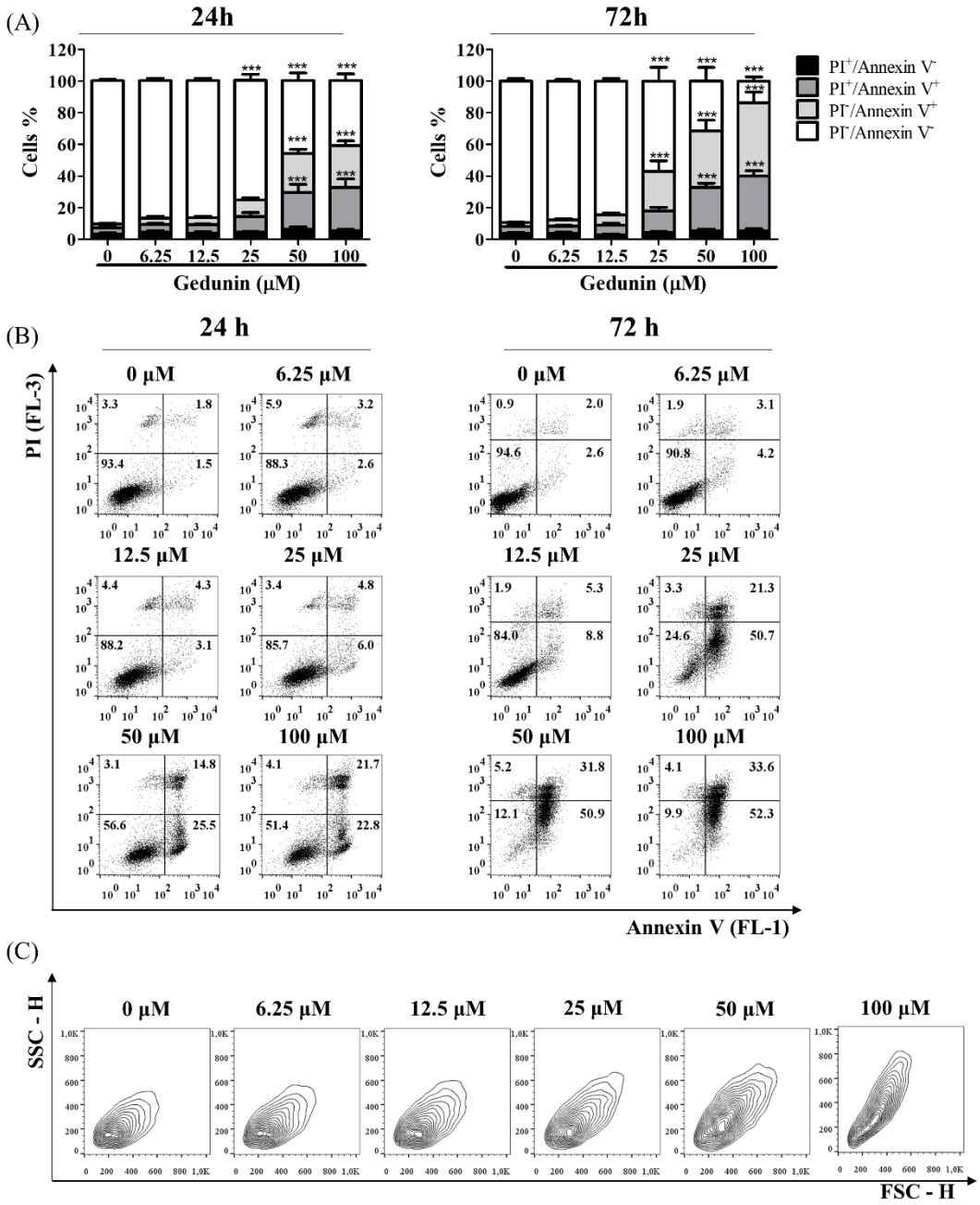

Figure 2. *Gedunin induces time- and concentration-dependent GL261 apoptosis.* (A) Effect of gedunin (6.25-100 µM) on GL261 cell (2×10^4/well) apoptosis evaluated by propidium iodide and annexin V-FITC staining MTT (FacsCalibur – BD Biosciences) 24 h and 72 h after incubation. Results are expressed as the mean ± SEM of viability percentage from triplicates wells from three independent experiments (24 well plates). * indicates statistically significant differences ($p \leq 0.05$) between treated and untreated cells. (B) Representative dot plots of flow cytometry analysis of gedunin-treated GL261 cells labeled with annexin V-FITC and PI after 24 and 72 h incubation. (C) Representative

411 contour plots of SSC-H and FSC-H of gedunin-treated (6.25 - 100 μM) GL261 cells after
412 72 h.
413

414 ***3.3 Gedunin impairs GL261 cell migration and invasiveness in vitro***

415 Tumor cell migration is an earlier step in cancer dissemination and invasion [58,59].
416 Scratch assay shows that gedunin (12.5 and 25 μM) reduced GL261 cell migration when
417 compared to the untreated group within 24 h, 48 h, and 72 h (**Fig. 3A, B**). Confirming
418 results obtained in the scratch assay, reduction of chemotaxis was also observed in the
419 Boyden chamber migration assay, in which gedunin treatment (25 μM) impaired cell
420 migration within 48 h (**Fig. 3C**).

421 Extracellular matrix remodeling by the proteolytic activity of tumor cell matrix
422 metalloproteinases (MMPs) is a crucial step for tumor cell invasion in the surrounding
423 tissue [60]. Gedunin also reduced the activity of MMP-2 (**Fig. 3D**), suggesting that this
424 limonoid impairs different mechanisms associated with tumor cell invasion.
425

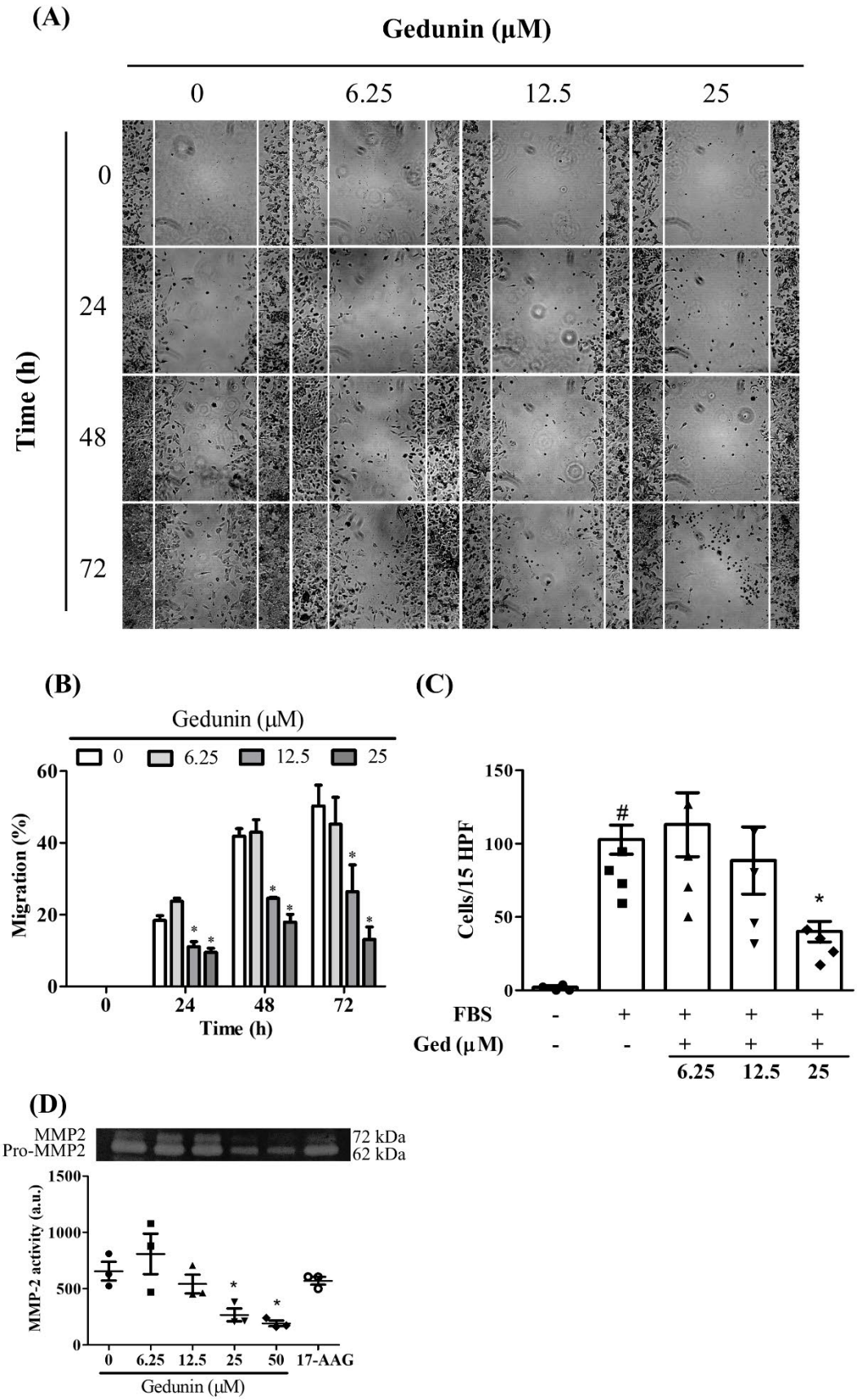
(A)
Gedunin (μM)
0
6.25
12.5
25
Time (h)
0
24
48
72
(B)
Gedunin (μM)
0
6.25
12.5
25
Migration (%)
Time (h)
(C)
Cells/15 HPF
FBS
Ged (μM)
6.25
12.5
25
(D)
MMP2
Pro-MMP2
72 kDa
62 kDa
MMP-2 activity (a.u.)
17-AAG
Gedunin (μM)

426

427
428 **Figure 3.** *Gedunin impairs in vitro GL261 cell migration and invasiveness.* (A)
429 Microscopic views of *the in vitro* scratch assay. GL261 migration into the scratched area
430 24-72 h after gedunin treatment (6.25-25 µM). (B) Percentages of GL261 cell migration
431 calculated as the ratio of uncovered area (24-72 h) by the initial scratched area (0 h).
432 Results are expressed as the mean ± SEM from two independent experiments (6 well
433 plates). (C) Boyden chamber chemotaxis assay demonstrating the number of gedunin-
434 treated or untreated cells per 15 high power fields (HPF) after 24 h migration. Results are
435 expressed as the mean ± SEM from quadruplicate wells. (D) MMP-2 activity of GL261
436 cell supernatant assessed by zymography assay 48 h after gedunin treatment (6.25-50
437 µM). Results are expressed as the mean ± SEM from two independent experiments. *
438 Indicates statistically significant differences ($p \leq 0.05$) between treated and untreated
439 cells, whereas # indicates statistically significant differences ($p \leq 0.05$) between
440 stimulated and unstimulated cells. FBS: fetal bovine serum.
441
442 ***3.4 Gedunin modulates signaling proteins in GL261 cells***
443 Ras/ERK is one of the main pro-survival pathways in glioblastoma cells [61,62].
444 Phosphorylation of ERK 1/2 (pERK) was induced by gedunin **(Fig. 4A-C**) whereas the
445 immunostaining of total ERK1/2 was reduced **(Fig. 4D**). It is noteworthy that the staining
446 of GAPDH, used as loading control, was also reduced (**Fig. 4A**; replicates in **Suppl. Fig.**
447 **3**) which may be explained by the induction of apoptosis and cell death. GL261 treatment
448 with 17-AAG also reduced total protein content but did not induce ERK phosphorylation
449 within the 24 h incubation.
450
451
452
453
454
455
456
457
458
459
460

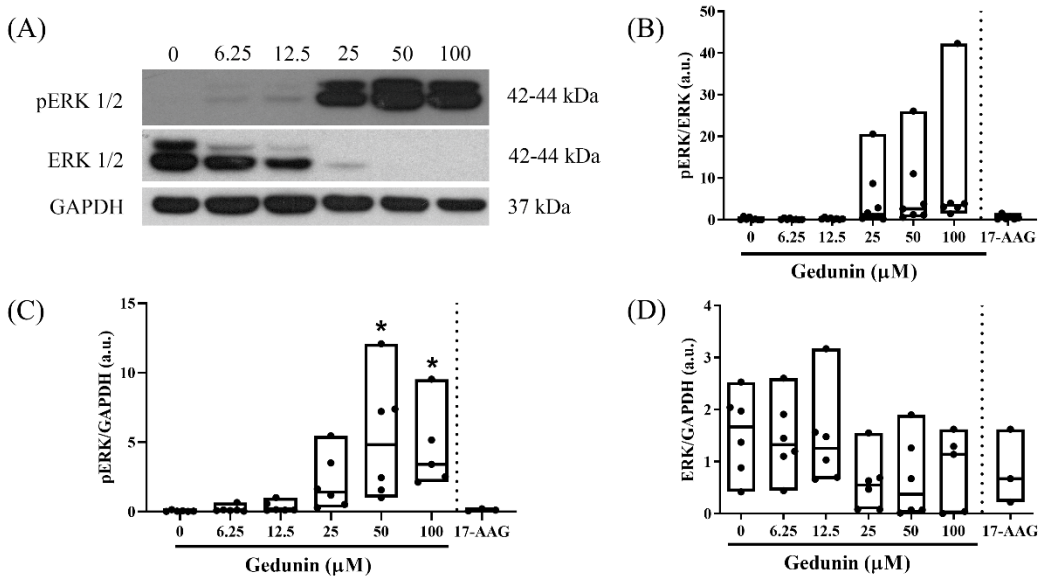

461 **Figure 4.** *Gedunin activates ERK 1/2 pathway.* Western blot analysis of the effect of
462 gedunin (6.25 – 100 μM) on intracellular signaling proteins, 24 h after treatment. (A)
463 Representative immunoblots of one experiment out of 8 independent experiments with a
464 similar trend. Box plots of (B) pERK/ERK, (C) pERK/GAPDH and (D) ERK/GAPDH
465 on GL261 cells. 17-AAG was used as the reference control of HSP90 activity inhibition.
466 GAPDH was used as the loading control. Results are expressed as the mean ± SEM of
467 protein expression from six independent experiments. * indicates statistically significant
468 differences ($p \leq 0.05$) between treated and untreated cells. Please find the uncropped blots
469 in supplemental figure 3.
470

471 ***3.5 Gedunin effect on glioblastoma in vivo***

472 The orthotopic C57BL/6 mouse glioblastoma model used in the present study has been
473 established as a standard procedure to reproduce human molecular and histological
474 features of glioblastoma [63,64]. Biodistribution data obtained by our group show that
475 ^{99m}Tc-labeled-gedunin did not reach substantial levels in the brain tissue when
476 intravenously injected in mice (Costa et al., *manuscript in preparation*). We, therefore,
477 assessed whether gedunin *in vivo* treatment was effective by using osmotic pumps placed
478 *in situ.*

479 Computed tomography (CT) scans revealed solid tumor growth that occupied an
480 extensive area of the brain tissue of mice from all groups (white mass, top panels in
481 black background of **Fig. 5A,** indicated by an asterisk in the upper left image scan).
482 Three-dimensional reconstructions of CT images are shown in **Figure 5** bottom panels,
483 in which tumor mass is represented by white over gray (brain) areas. Even though tumor
484 volume median values (mm^3) of gedunin-treated mice were smaller than those for
485 untreated or DMSO-injected mice, variability within groups was high (lowest and
486 highest tumor volume values for each group were: untreated, 21.7 - 75.6; DMSO, 16.8 -
487 83.6; GED, 11.7 - 67.4). No significant differences were observed between groups
488 (ANOVA, $p = 0.106$; **Fig. 5B, C**). **Supplemental Figure 4** shows CT of mouse brains
489 with and without tumors, for a better illustration of the tumor mass. Body mass (g) was
490 measured before GL261 injection and 28 days later, and no alterations were observed
491 (data not shown).

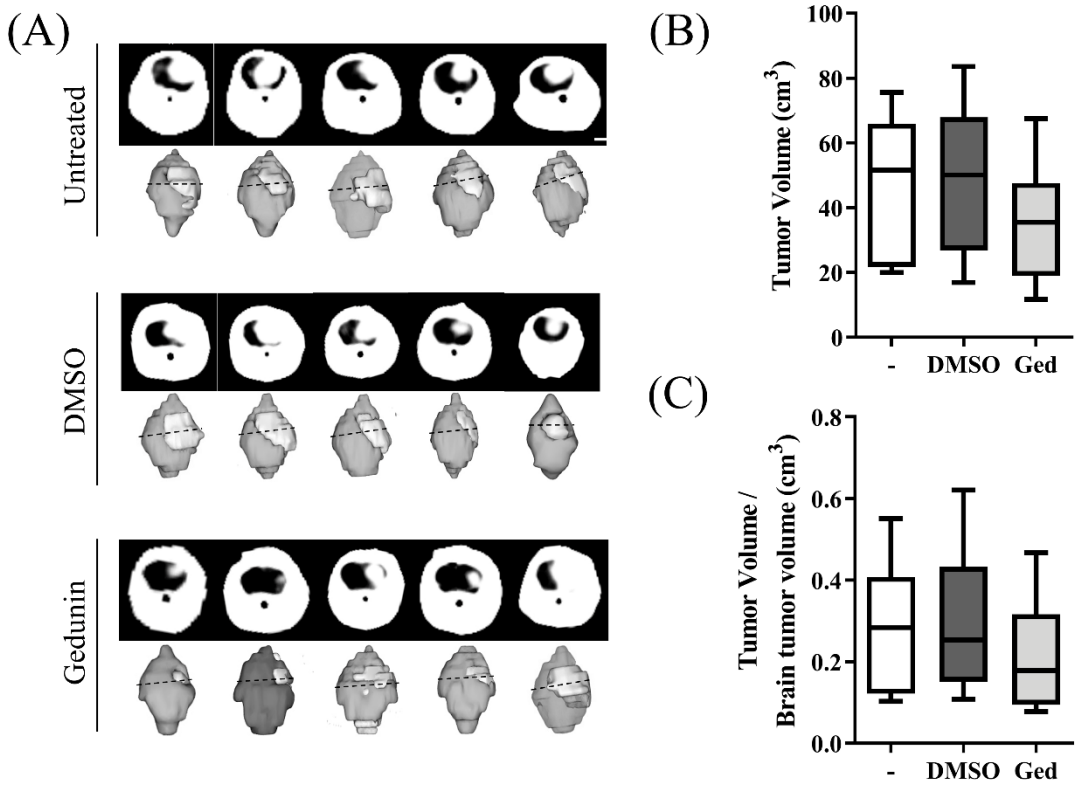

492

493 **Figure 5.** *Tumor size analysis of gedunin-treated mice.* (A) Representative sequential
494 coronal CT-images and respective 3D brain reconstructions (dorsal view) from untreated,
495 DMSO-injected and gedunin (250 μM)-treated mice. Lighter regions in 3D
496 reconstructions represent brain tumors. Images were acquired after 14 days of *in situ*
497 treatment (Alzet® osmotic minipumps) in GL261 cell-injected mice (1×10^5 cells/brain/2
498 μL). Boxplot graphs show tumor volume values (B) and the ratio between tumor and
499 mouse brain volume values (C) from 6-8 mice per group out of 2 independent
500 experiments. Tumor volumetry was determined by selecting contrast-enhanced regions
501 of interest in coronal sections using InVesalius 3.1.1 software. CT: Computed
502 Tomography. The white area corresponds to the glioblastoma observed in all CT scans.
503 Dashed line: coronal slice cut point. Results are expressed as the mean ± SEM of tumor
504 volume measurements from two independent experiments.
505

506 Because clinical CT scanners are designed for imaging human brains, which have
507 volumes roughly 3,000 times larger than those of mice [65–67], the limited spatial
508 resolution may not be precise enough to reliably assess treatment responses in small
509 murine brains [68,69]. To address this limitation, we investigated whether differences
510 between groups could be detected by analyzing tumor area from histological sections.
511 Indeed, **Figure 6** illustrates that gedunin-treated mice had reduced tumor central area (see

512 Methods section). In addition, gedunin-treated brain tumors displayed fewer vascular
513 structures **(Table 1 and Supplemental Figure 5).**

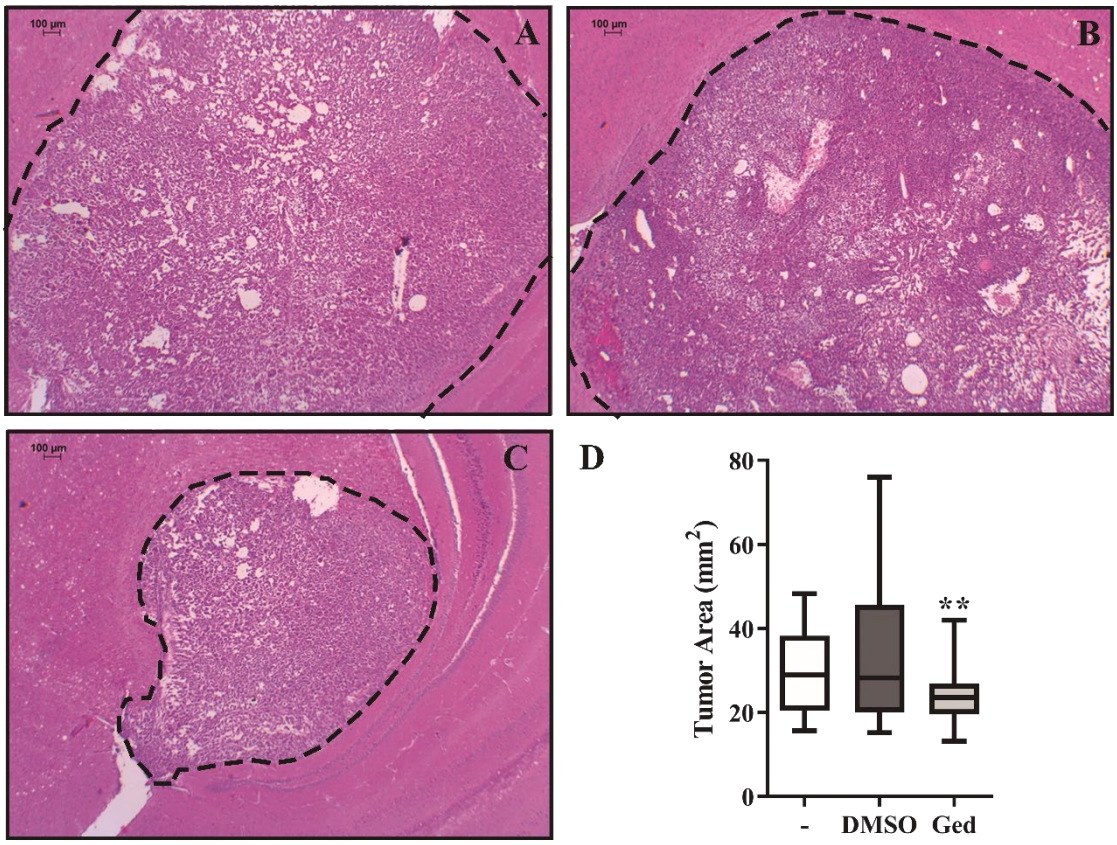

514

515 **Figure 6.** *Tumor size analysis of gedunin-treated mice.* Representative images of coronal
516 mouse brain slices stained with hematoxylin and eosin showing the tumor central area
517 (100 × magnification) of (A) untreated, (B) DMSO-, and (C) gedunin-treated mice (n=8
518 per group) 28 days after GL261 cell implantation. (D) Boxplot graph displaying tumor
519 central area values measured in histological brain sections. Results are expressed as the
520 mean ± SEM of tumor central area measurements from two independent experiments.
521 ** Indicates statistically significant differences ($p \leq 0.05$) between gedunin-treated and
522 DMSO-treated cells.

523

524

525 **Table 1**. **Glioblastoma histology features after gedunin *in vivo* treatment**

	Untreated	DMSO	Gedunin	p
Vascular Structures	13	32	8	P< 0.05 *
Liquefactive Necrosis	9.6%	10.6%	8.8%	NS
Intratumoral Hemorrhage	+	++	++	NS

Mitosis	+	++	+	NS

Table 1. *Glioblastoma histology features after gedunin in vivo treatment.* Table shows absolute and semi-quantitative description of the histological analyses of brain slices and p-values of gedunin-treated vs DMSO-treated mice, analyzed by Tukey's post-test. NS= non-significant; += discrete; ++= moderate.

4. Discussion

Uncontrolled proliferation and apoptosis resistance are central features of tumor development, being major targets for cancer treatment [19]. HSP90 is a key factor for tumor growth, since it chaperones several essential proteins involved in oncogenic processes. In the present study, we demonstrate that gedunin, a natural occurring HSP90 inhibitor, impairs murine glioblastoma cell growth *in vitro*, by arresting proliferation and inducing cell death in non-toxic concentrations to primary mouse brain cells. As previously shown in human cell lines [43,44], gedunin reduced murine glioblastoma cell migration, tumor-related signaling pathways, and extracellular metalloproteinase MMP-2 activity, features involved in glioblastoma growth. GL261-orthotopically injected C57BL/6 mice treated with gedunin had reduced presence of vascular structures, an important hallmark of tumor maintenance and growth.

Gedunin and other HSP90-binding agents induce the expression of HSP70 in cancer cells due to HSP90 inhibition (**Suppl. Figure 6**) [70–72] and show antiproliferative and cytotoxic effects against different tumor cells [37,39–42]. HSP90 inhibitors have increased affinity to the HSP90 machinery expressed by tumor cells [16]. This supports our data showing that gedunin toxicity against GL261 cells was achieved at a concentration lower than half of the required against primary glial cells [73]. Gedunin-triggered apoptosis, detected by phosphatidylserine exposure on the cell surface, was confirmed by flow cytometric analysis of cell physical criteria that showed the reduced size and increased granularity of apoptotic cells, due to the formation of apoptotic bodies and plasma membrane blebbing [55]. Our results clearly show that, as apoptosis progresses, GL261 cell FSC becomes progressively lower (likely due to cell dehydration and shrinkage), whereas SSC increases, due to cytoplasm and nuclear condensation [55,57].

Glioblastoma is a highly invasive and diffuse tumor that requires cell migration and extracellular matrix degradation to spread to adjacent tissue [74,75]. Scratch and

558 chemotaxis assays showed that gedunin diminished GL261 migration, in concentrations
559 and time points lower than the ones that induced cytotoxicity. Another way by which
560 gedunin controls tumor invasiveness is by inhibiting MMP-2 activity, with a higher effect
561 than 17-AAG. Indeed, HSP90 stabilizes and promotes the activation of extracellular
562 MMP-2, being crucial for GL261 and HT-1080 tumor cell invasion [76,77].

563 Although total ERK ½ was reduced, gedunin promoted a strong sustained (24 h) ERK1/2
564 activation/phosphorylation, corroborating previous work which demonstrate that HSP90
565 inhibition can also prompt the phosphorylation/activation of ERK [78,79]. The activation
566 of ERK ½ pathway is associated with mechanisms involved in GBM development such
567 as proliferation, invasion, metabolism, and death [80,81]. However, depending on the cell
568 type and stimulus, ERK ½ sustained activation can promote cell cycle arrest, autophagic
569 vacuolization, or caspase activation leading to cell senescence, autophagy, or apoptosis,
570 respectively [82–84], mechanisms that might be involved in the reduced levels of GL261
571 cell proliferation, migration, and induced programmed cell death observed in this work.

572 As previously mentioned in the results section, even though our findings indicate that
573 gedunin fits the predicted ADMET criteria for druggability and BBB permeation,
574 systemic (i.v.) administration of ^{99m}TC-labeled gedunin failed to reach the brain tissue at
575 substantial levels (Costa *et al*., manuscript in preparation). Hence, we used gedunin-filled
576 Alzet® minipumps to perform *in situ* treatment (resembling the FDA-approved Gliadel®
577 [carmustine] implants) to ensure that gedunin would be available at the tumor site. It is
578 important to note that the residual volume of gedunin inside the minipumps was measured
579 at the end of treatment to ensure that gedunin was released *in situ* (values shown in **Suppl.**
580 **Table 1**). It is important to emphasize the limitations of the CT mouse brain image
581 acquisition using a clinical CT scanner, since the limited spatial resolution of clinical CT
582 scanners might not be precise enough to analyze such a small brain [68,69]. While our
583 findings reinforce the feasibility of using clinical CT scanners for *in vivo* brain tumor
584 imaging in mice, their use for detecting treatment responses in tumor volume requires
585 further investigation. Another limitation of our study is that mouse tumor sizes were not
586 evaluated over time, since CT scan was only feasible in mice with no minipump implants,
587 due to the stainless steel of brain infusion cannulas.
588 As expected, GL261-injections triggered the development of mouse glioblastoma in
589 orthotopically-injected C57BL/6 mice with liquefactive necrosis, hemorrhage, mitosis,

590 and increased vascular structures [63]. *In situ* treatment with gedunin significantly
591 reduced tumor central area and the presence of vascular structures, which might decrease
592 tumor nutritional supply.
593 The severity and the poor prognosis of patients bearing glioblastoma call for new
594 therapeutic targets and drugs. Data presented in this paper sheds light on alternative
595 treatments for this type of tumor by revealing GL261 dependency of HSP90 and gedunin
596 as a potential lead compound.
597
598 ***Funding***
599 This work was supported by the Carlos Chagas Filho Research Support Foundation
600 (FAPERJ), the Coordination for the Improvement of Higher Education Personnel
601 (CAPES), the Brazilian agency National Council for Scientific and Technological
602 Development (CNPq), and the Oswaldo Cruz Foundation (Fiocruz). CP, MGMO, and
603 ACM hold fellowships from CNPq. TEMMC was a PhD student from the Graduate
604 Program in Cell and Molecular Biology (IOC/Fiocruz).
605
606 ***Conflict of interest***
607 The authors declare no conflict of interest.
608
609 ***Author contributions***
610 CP, TEMMC, and TEK conceived and designed the work. TEMMC, CP, TEK, ACM,
611 and MGH designed experiments. TEMMC, CP, TAP, LNS, EMC, CCF, CMMM, JXP,
612 VGR, YAV, and TEK performed the experiments, acquired, and/or analyzed data. CP,
613 TEK, ACM, JXC, and MGH contributed with funding and resources. CP supervised the
614 work. CP and TEMMC wrote the original draft. CMMM and TEK wrote and revised the
615 manuscript. All authors revised and edited the final manuscript.
616
617 ***Acknowledgments***
618 The authors gratefully acknowledge Dr. André Luis Peixoto Candéa, D.Sc. Erika Tatiana
619 Muñoz, Dr. Samara Cristina Ferreira Machado, Edson Santos Silva, Filipe Leal Portilho,
620 Ubirajara Ribeiro, and Maria Heloisa Oliveira for technical support. We also thank the

Institute for Biomodels Science and Technology (Fiocruz) for providing mice, and the Center for Cancer Control (CUCC, UERJ) for the help with CT imaging acquisition.

References

[1] Louis DN, Perry A, Reifenberger G, Deimling AV, Figarella D, Webster B, et al. The 2016 World Health Organization Classification of Tumors of the Central Nervous System : a summary. Acta Neuropathol (Berl) 2016. https://doi.org/10.1007/s00401-016-1545-1.

[2] Ostrom QT, Price M, Neff C, Cioffi G, Waite KA, Kruchko C, et al. CBTRUS Statistical Report: Primary Brain and Other Central Nervous System Tumors Diagnosed in the United States in 2016—2020. Neuro-Oncol 2023;25:iv1–99. https://doi.org/10.1093/neuonc/noad149.

[3] Delgado-López PD, Corrales-García EM. Survival in glioblastoma: a review on the impact of treatment modalities. Clin Transl Oncol 2016;18:1062–71. https://doi.org/10.1007/s12094-016-1497-x.

[4] Stupp R, Mason WP, van den Bent MJ, Weller M, Fisher B, Taphoorn MJ, et al. Radiotherapy plus concomitant and adjuvant temozolomide for glioblastoma. N Engl J Med 2005;352:987–96. https://doi.org/10.1056/NEJMoa043330.

[5] Niewald M, Berdel C, Fleckenstein J, Licht N, Ketter R, Rübe C. Toxicity after radiochemotherapy for glioblastoma using temozolomide - a retrospective evaluation. Radiat Oncol 2011;6:141. https://doi.org/10.1186/1748-717X-6-141.

[6] Dinnes J, Cave C, Huang S, Milne R. A rapid and systematic review of the effectiveness of temozolomide for the treatment of recurrent malignant glioma. Br J Cancer 2002;86:501–5. https://doi.org/10.1038/sj.bjc.6600135.

[7] Attarian F, Taghizadeh-Hesary F, Fanipakdel A, Javadinia SA, Porouhan P, PeyroShabany B, et al. A Systematic Review and Meta-Analysis on the Number of Adjuvant Temozolomide Cycles in Newly Diagnosed Glioblastoma. Front Oncol 2021;11:1–6. https://doi.org/10.3389/fonc.2021.779491.

[8] Lechapt-Zalcman E, Levallet G, Dugué AE, Vital A, Diebold M-D, Menei P, et al. O6-methylguanine-DNA methyltransferase (MGMT) promoter methylation and low MGMT-encoded protein expression as prognostic markers in glioblastoma patients treated with biodegradable carmustine wafer implants after initial surgery followed by radiotherapy w. Cancer 2012;118:4545–54. https://doi.org/10.1002/cncr.27441.

[9] Jena Lynnand McErlean E and MH, Jena L, McErlean E, McCarthy H. Delivery across the blood-brain barrier: nanomedicine for glioblastoma multiforme. Drug Deliv Transl Res 2020;10:304–18. https://doi.org/10.1007/s13346-019-00679-2.

[10] McGirt MJ, Than KD, Weingart JD, Chaichana KL, Attenello FJ, Olivi A, et al. Gliadel (BCNU) wafer plus concomitant temozolomide therapy after primary resection of glioblastoma multiforme. J Neurosurg JNS 2009;110:583–8. https://doi.org/10.3171/2008.5.17557.

[11] Qi Z, Xing W, Shao C, Yang C, Wang Z. The role of Gliadel wafers in the treatment of newly diagnosed GBM: a meta-analysis. Drug Des Devel Ther 2015;9:3341. https://doi.org/10.2147/DDDT.S85943.

666 [12] Reithmeier T, Graf E, Piroth T, Trippel M, Pinsker MO, Nikkhah G. BCNU for
667 recurrent glioblastoma multiforme: efficacy, toxicity and prognostic factors. BMC
668 Cancer 2010;10:30. https://doi.org/10.1186/1471-2407-10-30.
669 [13] Bregy A, Shah AH, Diaz MV, Pierce HE, Ames PL, Diaz D, et al. The role of
670 Gliadel wafers in the treatment of high-grade gliomas. Expert Rev Anticancer Ther
671 2013;13:1453–61. https://doi.org/10.1586/14737140.2013.840090.
672 [14] Alexandru O, Purcaru S, Tataranu L, Lucan L, Castro J, Folcuţi C, et al. The
673 Influence of EGFR Inactivation on the Radiation Response in High Grade Glioma. Int J
674 Mol Sci 2018;19:229. https://doi.org/10.3390/ijms19010229.
675 [15] Tanaka S, Louis DN, Curry WT, Batchelor TT, Dietrich J. Diagnostic and
676 therapeutic avenues for glioblastoma : no longer a dead end ? Nat Rev Clin Oncol
677 2012;10:14–26. https://doi.org/10.1038/nrclinonc.2012.204.
678 [16] Trepel J, Mollapour M, Giaccone G, Neckers L. Targeting the dynamic HSP90
679 complex in cancer. Nat Rev Cancer 2010;10:537–49. https://doi.org/10.1038/nrc2887.
680 [17] Sasame J, Ikegaya N, Kawazu M, Natsumeda M, Hayashi T, Isoda M, et al.
681 HSP90 Inhibition Overcomes Resistance to Molecular Targeted Therapy in
682 BRAFV600E-mutant High-grade Glioma. Clin Cancer Res 2022;28:2425–39.
683 https://doi.org/10.1158/1078-0432.CCR-21-3622.
684 [18] Wei S, Yin D, Yu S, Lin X, Savani MR, Du K, et al. Antitumor Activity of a
685 Mitochondrial-Targeted HSP90 Inhibitor in Gliomas. Clin Cancer Res 2022;28:2180–
686 95. https://doi.org/10.1158/1078-0432.CCR-21-0833.
687 [19] Hanahan D. Hallmarks of Cancer: New Dimensions. Cancer Discov
688 2022;12:31–46. https://doi.org/10.1158/2159-8290.CD-21-1059.
689 [20] Cheng Q, Chang JT, Geradts J, Neckers LM, Haystead T, Spector NL, et al.
690 Amplification and high-level expression of heat shock protein 90 marks aggressive
691 phenotypes of human epidermal growth factor receptor 2 negative breast cancer. Breast
692 Cancer Res 2012;14:R62. https://doi.org/10.1186/bcr3168.
693 [21] Kubota H, Yamamoto S, Itoh E, Abe Y, Nakamura A, Izumi Y, et al. Increased
694 expression of co-chaperone HOP with HSP90 and HSC70 and complex formation in
695 human colonic carcinoma. Cell Stress Chaperones 2010;15:1003–11.
696 https://doi.org/10.1007/s12192-010-0211-0.
697 [22] McCarthy MM, Pick E, Kluger Y, Gould-Rothberg B, Lazova R, Camp RL, et
698 al. HSP90 as a marker of progression in melanoma. Ann Oncol 2008;19:590–4.
699 https://doi.org/10.1093/annonc/mdm545.
700 [23] Pick E, Kluger Y, Giltnane JM, Moeder C, Camp RL, Rimm DL, et al. High
701 HSP90 expression is associated with decreased survival in breast cancer. Cancer Res
702 2007;67:2932–7. https://doi.org/10.1158/0008-5472.CAN-06-4511.
703 [24] Schopf FH, Biebl MM, Buchner J. The HSP90 chaperone machinery. Nat Rev
704 Mol Cell Biol 2017;18:345–60. https://doi.org/10.1038/nrm.2017.20.
705 [25] Fukuyo Y, Hunt CR, Horikoshi N. Geldanamycin and its anti-cancer activities.
706 Cancer Lett 2010;290:24–35. https://doi.org/10.1016/j.canlet.2009.07.010.
707 [26] Blagosklonny MV. Hsp-90-associated oncoproteins: Multiple targets of
708 geldanamycin and its analogs. Leukemia 2002;16:455–62.
709 https://doi.org/10.1038/sj.leu.2402415.
710 [27] Gaspar N, Sharp SY, Eccles SA, Gowan S, Popov S, Jones C, et al. Mechanistic
711 evaluation of the novel HSP90 inhibitor NVP-AUY922 in adult and pediatric
712 glioblastoma. Mol Cancer Ther 2010;9:1219–33. https://doi.org/10.1158/1535-
713 7163.MCT-09-0683.

714 [28] Newman B, Liu Y, Lee HF, Sun D, Wang Y. HSP90 inhibitor 17-AAG
715 selectively eradicates lymphoma stem cells. Cancer Res 2012;72:4551–61.
716 https://doi.org/10.1158/0008-5472.CAN-11-3600.
717 [29] Eccles SA, Massey A, Raynaud FI, Sharp SY, Box G, Valenti M, et al. NVP-
718 AUY922: a novel heat shock protein 90 inhibitor active against xenograft tumor growth,
719 angiogenesis, and metastasis. Cancer Res 2008;68:2850–60.
720 https://doi.org/10.1158/0008-5472.CAN-07-5256.
721 [30] Kim HB, Lee SH, Um JH, Oh WK, Kim DW, Kang CD, et al. Sensitization of
722 multidrug-resistant human cancer cells to Hsp90 inhibitors by down-regulation of
723 SIRT1. Oncotarget 2015;6:36202–18. https://doi.org/10.18632/oncotarget.5343.
724 [31] Shimamura T, Perera SA, Foley KP, Sang J, Rodig SJ, Inoue T, et al.
725 Ganetespib (STA-9090), a nongeldanamycin HSP90 inhibitor, has potent antitumor
726 activity in in vitro and in vivo models of non-small cell lung cancer. Clin Cancer Res
727 2012;18:4973–85. https://doi.org/10.1158/1078-0432.CCR-11-2967.
728 [32] Clinical Trials 2020.
729 https://clinicaltrials.gov/ct2/results?cond=Cancer&term=HSP90+inhibitor&cntry=&stat
730 e=&city=&dist=.
731 [33] Solit DB, Ivy SP, Kopil C, Sikorski R, Morris MJ, Slovin SF, et al. Cancer
732 Therapy : Clinical Phase I T rial of 17-Allylamino-17-Demethoxygeldanamycin in
733 Patients with Advanced Cancer 2007;13:1775–82. https://doi.org/10.1158/1078-
734 0432.CCR-06-1863.
735 [34] Zhou D, Liu Y, Ye J, Ying W, Ogawa LS, Inoue T, et al. A rat retinal damage
736 model predicts for potential clinical visual disturbances induced by Hsp90 inhibitors.
737 Toxicol Appl Pharmacol 2013;273:401–9. https://doi.org/10.1016/j.taap.2013.09.018.
738 [35] Hallur G, Sivramakrishnan A, Bhat SV. Three New Tetranortriterpenoids from
739 Neem Seed Oil. J Nat Prod 2002;65:1177–9. https://doi.org/10.1021/np0105174.
740 [36] Brandt GEL, Schmidt MD, Prisinzano TE, Blagg BSJ. Gedunin, a novel hsp90
741 inhibitor: semisynthesis of derivatives and preliminary structure-activity relationships. J
742 Med Chem 2008;51:6495–502. https://doi.org/10.1021/jm8007486.
743 [37] Patwardhan CA, Fauq A, Peterson LB, Miller C, Blagg BSJ, Chadli A. Gedunin
744 inactivates the co-chaperone p23 protein causing cancer cell death by apoptosis. J Biol
745 Chem 2013;288:7313–25. https://doi.org/10.1074/jbc.M112.427328.
746 [38] Matts RL, Brandt GEL, Lu Y, Dixit A, Mollapour M, Wang S, et al. A
747 systematic protocol for the characterization of Hsp90 modulators. Bioorg Med Chem
748 2011;19:684–92. https://doi.org/10.1016/j.bmc.2010.10.029.
749 [39] Subramani R, Gonzalez E, Nandy SB, Arumugam A, Camacho F, Medel J, et al.
750 Gedunin inhibits pancreatic cancer by altering sonic hedgehog signaling pathway.
751 Oncotarget 2017;8:10891–904. https://doi.org/10.18632/oncotarget.8055.
752 [40] Kamath SG, Chen N, Xiong Y, Wenham R, Apte S, Humphrey M, et al.
753 Gedunin, a novel natural substance, inhibits ovarian cancer cell proliferation. Int J
754 Gynecol Cancer 2009;19:1564–9. https://doi.org/10.1111/IGC.0b013e3181a83135.
755 [41] Uddin SJ, Nahar L, Shilpi JA, Shoeb M, Borkowski T, Gibbons S, et al.
756 Gedunin, a limonoid from Xylocarpus granatum, inhibits the growth of CaCo-2 colon
757 cancer cell line in vitro. Phytother Res 2007;21:757–61.
758 https://doi.org/10.1002/ptr.2159.
759 [42] Kishore T KK, Ganugula R, Gade DR, Reddy GB, Nagini S. Gedunin abrogates
760 aldose reductase, PI3K/Akt/mToR, and NF-κB signaling pathways to inhibit

761 angiogenesis in a hamster model of oral carcinogenesis. Tumor Biol 2016;37:2083–93.
762 https://doi.org/10.1007/s13277-015-4003-0.
763 [43] Li H, Wu JG, Zhang HW, Wang W, Zhang YX, Zhang JN. Inhibition of
764 proliferation, invasion and migration in U-251 MG glioblastoma cell line by gedunin.
765 Int J Pharmacol 2018. https://doi.org/10.3923/ijp.2018.522.527.
766 [44] Stouffer M, Wandling E, Dickson L, Lin S, Duan H, Powe E, et al. Gedunin
767 modulates cellular growth and apoptosis in glioblastoma cell lines. Cancer Rep
768 2024;7:e2051. https://doi.org/10.1002/cnr2.2051.
769 [45] Kilkenny C, Browne WJ, Cuthill IC, Emerson M, Altman DG. Improving
770 Bioscience Research Reporting: The ARRIVE Guidelines for Reporting Animal
771 Research. PLOS Biol 2010;8:e1000412. https://doi.org/10.1371/journal.pbio.1000412.
772 [46] Schneider CA, Rasband WS, Eliceiri KW. NIH Image to ImageJ: 25 years of
773 image analysis. Nat Methods 2012;9:671–5. https://doi.org/10.1038/nmeth.2089.
774 [47] Liang C-C, Park AY, Guan J-L. In vitro scratch assay: a convenient and
775 inexpensive method for analysis of cell migration in vitro. Nat Protoc 2007;2:329–33.
776 https://doi.org/10.1038/nprot.2007.30.
777 [48] Esteve PO, Tremblay P, Houde M, St-Pierre Y, Mandeville R. In vitro
778 expression of MMP-2 and MMP-9 in glioma cells following exposure to inflammatory
779 mediators. Biochim Biophys Acta - Mol Cell Res 1998;1403:85–96.
780 https://doi.org/10.1016/S0167-4889(98)00020-2.
781 [49] Cha S, Johnson G, Wadghiri YZ, Jin O, Babb J, Zagzag D, et al. Dynamic ,
782 Contrast-Enhanced Perfusion MRI in Mouse Gliomas : Correlation With
783 Histopathology 2003;855:848–55. https://doi.org/10.1002/mrm.10446.
784 [50] Paxinos G, Franklin KBJ. The mouse brain in stereotaxic coordinates: hard
785 cover edition. Acad Press 2001;2nd Editio:360.
786 [51] CCAC GUIDELINES. Can Vet J 2003;44:631.
787 [52] Pereira JX, Azeredo MCB, Martins FS, Chammas R, Oliveira FL, Santos SN, et
788 al. The deficiency of galectin-3 in stromal cells leads to enhanced tumor growth and
789 bone marrow metastasis. BMC Cancer 2016;16:636. https://doi.org/10.1186/s12885-
790 016-2679-1.
791 [53] Vermes I, Haanen C, Steffens-Nakken H, Reutellingsperger C. A novel assay for
792 apoptosis Flow cytometric detection of phosphatidylserine expression on early apoptotic
793 cells using fluorescein labelled Annexin V. J Immunol Methods 1995;184:39–51.
794 https://doi.org/10.1016/0022-1759(95)00072-I.
795 [54] Barroso G, Taylor S, Morshedi M, Manzur F, Gaviño F, Oehninger S.
796 Mitochondrial membrane potential integrity and plasma membrane translocation of
797 phosphatidylserine as early apoptotic markers: a comparison of two different sperm
798 subpopulations. Fertil Steril 2006;85:149–54.
799 https://doi.org/10.1016/j.fertnstert.2005.06.046.
800 [55] Skommer J, Wlodkowic D, Telford W, Skommer J, Darzynkiewicz Z. Apoptosis
801 and beyond: cytometry in studies of programmed cell death. Methods Cell Biol
802 2011;103:55–98. https://doi.org/10.1016/B978-0-12-385493-3.00004-8.
803 [56] Schmid I, Uittenbogaart CH, Giorgi JV. Sensitive method for measuring
804 apoptosis and cell surface phenotype in human thymocytes by flow cytometry.
805 Cytometry 1994;15:12–20. https://doi.org/10.1002/cyto.990150104.
806 [57] Ormerod MG, Paul F, Cheetham M, Sun X -M. Discrimination of apoptotic
807 thymocytes by forward light scatter. Cytometry 1995;21:300–4.
808 https://doi.org/10.1002/cyto.990210311.

[58] Wells A, Grahovac J, Wheeler S, Ma B, Lauffenburger D. Targeting tumor cell motility as a strategy against invasion and metastasis. Trends Pharmacol Sci 2013;34:283–9. https://doi.org/10.1016/j.tips.2013.03.001.
[59] Eddy RJ, Weidmann MD, Sharma VP, Condeelis JS. Tumor Cell Invadopodia: Invasive Protrusions that Orchestrate Metastasis. Trends Cell Biol 2017;27:595–607. https://doi.org/10.1016/j.tcb.2017.03.003.
[60] Winkler J, Abisoye-Ogunniyan A, Metcalf KJ, Werb Z. Concepts of extracellular matrix remodelling in tumour progression and metastasis. Nat Commun 2020;11:5120. https://doi.org/10.1038/s41467-020-18794-x.
[61] Chen D, Zuo D, Luan C, Liu M, Na M, Ran L, et al. Glioma cell proliferation controlled by ERK activity-dependent surface expression of PDGFRA. PLoS ONE 2014;9. https://doi.org/10.1371/journal.pone.0087281.
[62] Frattini V, Trifonov V, Chan JM, Castano A, Lia M, Abate F, et al. The integrated landscape of driver genomic alterations in glioblastoma. Nat Genet 2013;45:1141–9. https://doi.org/10.1038/ng.2734.
[63] Miyai M, Tomita H, Soeda A, Yano H, Iwama T, Hara A, et al. Current trends in mouse models of glioblastoma. J Neurooncol 2017;135:423–32. https://doi.org/10.1007/s11060-017-2626-2.
[64] Newcomb EW, Zagzag D. CNS Cancer. CNS Cancer 2009:227–41. https://doi.org/10.1007/978-1-60327-553-8.
[65] Hofman MA. Size and Shape of the Cerebral Cortex in Mammals. Brain Behav Evol 1988;32:17–26. https://doi.org/10.1159/000116529.
[66] Hofman M. Evolution of the human brain: when bigger is better. vol. 8. 2014.
[67] Welch A, Mingarelli M, Riedel G, Platt B. Mapping changes in mouse brain metabolism with PET/CT. J Nucl Med Off Publ Soc Nucl Med 2013;54:1946–53. https://doi.org/10.2967/jnumed.113.121509.
[68] Palmowski K, Winz O, Rix A, Bzyl J, Behrendt FF, Verburg FA, et al. Accuracy of a clinical PET/CT vs. a preclinical μPET system for monitoring treatment effects in tumour xenografts. Eur J Radiol 2013;82:1318–24. https://doi.org/10.1016/j.ejrad.2013.01.028.
[69] Kirschner S, Mürle B, Felix M, Arns A, Groden C, Wenz F, et al. Imaging of Orthotopic Glioblastoma Xenografts in Mice Using a Clinical CT Scanner: Comparison with Micro-CT and Histology. PLoS One 2016;11:e0165994. https://doi.org/10.1371/journal.pone.0165994.
[70] Kudryavtsev VA, Khokhlova AV, Mosina VA, Selivanova EI, Kabakov AE. Induction of Hsp70 in tumor cells treated with inhibitors of the Hsp90 activity: A predictive marker and promising target for radiosensitization. PLOS ONE 2017;12:e0173640-.
[71] Bagatell R, Paine-Murrieta GD, Taylor CW, Pulcini EJ, Akinaga S, Benjamin IJ, et al. Induction of a Heat Shock Factor 1-dependent Stress Response Alters the Cytotoxic Activity of Hsp90-binding Agents1. Clin Cancer Res 2000;6:3312–8.
[72] Kelland LR, Sharp SY, Rogers PM, Myers TG, Workman P. DT-Diaphorase expression and tumor cell sensitivity to 17-allylamino, 17-demethoxygeldanamycin, an inhibitor of heat shock protein 90. J Natl Cancer Inst 1999;91:1940–9.
[73] BADISA RB, DARLING-REED SF, JOSEPH P, COOPERWOOD JS, LATINWO LM, GOODMAN CB. Selective Cytotoxic Activities of Two Novel Synthetic Drugs on Human Breast Carcinoma MCF-7 Cells. Anticancer Res 2009;29:2993 LP – 2996.

857 [74] Faisal SM, Comba A, Varela ML, Argento AE, Brumley E, Abel C, et al. The
858 complex interactions between the cellular and non-cellular components of the brain
859 tumor microenvironmental landscape and their therapeutic implications. vol. 12. 2022.
860 [75] Seker-Polat F, Pinarbasi Degirmenci N, Solaroglu I, Bagci-Onder T. Tumor Cell
861 Infiltration into the Brain in Glioblastoma: From Mechanisms to Clinical Perspectives.
862 Cancers 2022;14. https://doi.org/10.3390/cancers14020443.
863 [76] Newcomb EW, Lukyanov Y, Schnee T, Esencay M, Fischer I, Hong D, et al.
864 The geldanamycin analogue 17-allylamino-17-demethoxygeldanamycin inhibits the
865 growth of GL261 glioma cells in vitro and in vivo. Anticancer Drugs 2007;18:875–82.
866 https://doi.org/10.1097/CAD.0b013e3281430df8.
867 [77] Eustace BK, Sakurai T, Stewart JK, Yimlamai D, Unger C, Zehetmeier C, et al.
868 Functional proteomic screens reveal an essential extracellular role for hsp90 alpha in
869 cancer cell invasiveness. Nat Cell Biol 2004;6:507–14. https://doi.org/10.1038/ncb1131.
870 [78] Duron DI, Lei W, Barker NK, Stine C, Mishra S, Blagg BSJ, et al. Inhibition of
871 Hsp90 in the spinal cord enhances the antinociceptive effects of morphine by activating
872 an ERK-RSK pathway. Sci Signal 2020;13. https://doi.org/10.1126/scisignal.aaz1854.
873 [79] Streicher JM. The role of heat shock proteins in regulating receptor signal
874 transduction. Mol Pharmacol 2019;95:468–74. https://doi.org/10.1124/mol.118.114652.
875 [80] Lailler C, Louandre C, Morisse MC, Lhossein T, Godin C, Lottin M, et al.
876 ERK1/2 signaling regulates the immune microenvironment and macrophage recruitment
877 in glioblastoma. Biosci Rep 2019;39. https://doi.org/10.1042/BSR20191433.
878 [81] Zhuang S, Schnellmann RG. A death-promoting role for extracellular signal-
879 regulated kinase. J Pharmacol Exp Ther 2006;319:991–7.
880 https://doi.org/10.1124/jpet.106.107367.
881 [82] Hong SK, Wu PK, Park JI. A cellular threshold for active ERK1/2 levels
882 determines Raf/MEK/ERK-mediated growth arrest versus death responses. Cell Signal
883 2018;42:11–20. https://doi.org/10.1016/j.cellsig.2017.10.001.
884 [83] Cagnol S, Chambard JC. ERK and cell death: Mechanisms of ERK-induced cell
885 death - Apoptosis, autophagy and senescence. FEBS J 2010;277:2–21.
886 https://doi.org/10.1111/j.1742-4658.2009.07366.x.
887 [84] Cagnol S, Van Obberghen-Schilling E, Chambard JC. Prolonged activation of
888 ERK1,2 induces FADD-independent caspase 8 activation and cell death. Apoptosis
889 2006. https://doi.org/10.1007/s10495-006-4065-y.